D.V. Bandourin, V.F. Konoplyanikov, N.B. Skachkov

Jet energy scale setting with "$\gamma + Jet$" events at LHC energies. Generalities, selection rules

1. INTRODUCTION

Setting an absolute scale for a hadronic calorimeter (HCAL) is an important task for many of pp and $p\bar{p}$ collider experiments (see e.g. [1, 2]). There is a number of ATLAS and CMS publications on this subject where the application of different physical processes (like "$Z^0/\gamma + Jet$" and others) is discussed ([3–10]).

This paper is the first part of a set of publications on a detailed study of this problem. The main goal of this work is to find out the selection criteria for "$\gamma + Jet$" events that would lead to the most precise determination of transverse momentum of a jet, i.e. ${P_t}^{Jet}$, via assigning a photon ${P_t}^{\gamma}$ to a jet. We shall present here the results of event generation by using PYTHIA 5.7 [11]. Further development, based on the simulation of detector response with GEANT detector simulation packages will be presented in one of our next papers.

It should be also noted that here we consider the case of a low luminosity $L = 10^{33}\, cm^2 s^{-1}$ that is still quite sufficient to use much more restrictive cuts as well as new physical variables and, correspondingly, cuts on them (cluster suppression criterion, for instance) in comparison with those used in the previous experiments and to obtain a set of more clean "$\gamma + Jet$" events.

The Section 2 is an introduction to the problem. General features of the "$\gamma{+}Jet$" processes at LHC energies, that will be explored in this article and later papers, are presented here. In Section 2 we review possible sources of the ${P_t}^{\gamma}$ and ${P_t}^{Jet}$ disbalance in the final state and the ways of selecting those events where this disbalance has a minimal value.

In Section 3.1 we present definitions of P_t components of different objects that enter the balance equation illustrating the conservation law of the total P_t in any event.

Section 3.2 describes the criteria we have chosen to select "$\gamma + Jet$" events for the calibration procedure. "Cluster" (or mini–jet) suppression criterion (P_{tCUT}^{clust}) which has not been used in previous experiments is introduced here. Its important role will be illustrated in the following papers [12–15]. These clusters have a physical sense as a part of another new experimentally measurable quantity introduced here for the first time, namely, the sum of the $\vec{P_t}$ of all particles detectable in the $|\eta| < 5$ region which are out of the "$\gamma + Jet$" system (denoted as ${P_t}^{out}$).

Another new thing here is an introduction of a new physical object, named as an "isolated jet", i.e. the jet that does not have any noticeable P_t activity in some ring in $\eta - \phi$ space around it. In other words we will select some class of events having a total P_t activity inside the ring, $\Delta R = 0.3$, around this "isolated jet" within $2-5\%$ of jet P_t. In the following paper it will be shown that the number of events with such a clean topological structure would not be small at LHC energies (mainly due to the growth of luminosity).

Since the calibration is rather a practical than an academical task in all the following Sections, we present the values of rates for strict and weak cut values because their choice would be a matter of step-by-step collected statistics.

The justification of the variables and cuts introduced in Section 3 can be found in our papers [13–15]. In [15] we present the estimation of the efficiency of background suppression, that is, finally, the main guideline to establish the selection rules.

Section 4 will be devoted to the estimation of non-detectable neutrino contribution to ${P_t}^{Jet}$ as well as to studying the influence of the $|\eta| > 5$ region not covered by calorimeters or other detectors (that is the main source of ${P_t}^{miss} \equiv \not{E}_T$) on the total P_t balance in the event. The correlation of the upper cut on ${P_t}^{miss}$ with a mean value of P_t of neutrinos belonging to the jet P_t, i.e. $\langle P_{t(\nu)}^{Jet} \rangle$, will be considered here.

Since the results presented here have been obtained with PYTHIA simulation, we are planning to carry out the analogous estimation in the next papers but with another event generator.

2. GENERALITIES OF "$\gamma + Jet$" PROCESSES

2.1 Leading order picture

The idea of a hadronic calorimeter (HCAL) calibration by physical process "$pp \to \gamma + Jet$" was realized many times in different experiments (see recent papers [1, 2] and refs. there). It is based on the parton picture where two partons ($q\bar{q}$ or qg), supposed to be moving in different colliding nucleons with zero transverse momenta (with respect to the beam line), produce a photon, called a direct one, and a parton with balanced transverse momentum $\vec{P_t}^{part} = -\vec{P_t}^{\gamma}$. This picture corresponds to the leading order (LO) Feynman diagrams shown in Fig. 1 for the "Compton-like" process

$$qg \to q + \gamma \qquad (1a)$$

and for "annihilation" process

$$q\overline{q} \to g + \gamma, \qquad (1b)$$

respectively. The P_t of the "γ+parton" system produced in the final state should be equal to zero, i.e.

$$\vec{P_t}^{\gamma+part} = \vec{P_t}^{\gamma} + \vec{P_t}^{part} = 0. \qquad (2)$$

So, in this case one could expect that with a reasonable precision the transverse momentum of the jet produced by the final state parton (q or g) will be close in magnitude to the transverse momentum of the final state photon, i.e. $\vec{P_t}^{Jet} \approx -\vec{P_t}^{\gamma}$.

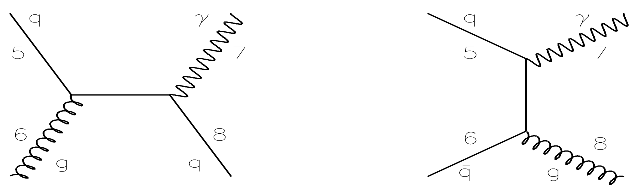

Fig. 1: Some of the leading order Feynman diagrams for direct photon production.

It allows one to carry out the calibration of HCAL in the experiments with a well calibrated electromagnetic calorimeter (ECAL). To put it simpler, to a part of jet transverse energy E_t^{Jet} deposited in HCAL we can assign the value of the difference between the value of the transverse energy deposited in ECAL in the photon direction, i.e. E_t^{γ}, and the value of the transverse energy deposited in ECAL in the jet direction.

2.2 Initial state radiation.

Since we believe in the perturbation theory, the leading order (LO) picture, described above, is expected to be dominant in determination of the main contribution to the cross section.

The Next-to-Leading Order (NLO) approximation (see some of the NLO diagrams in Fig. 2) introduces some deviations from a rather straightforward LO-motivated idea of calibration. Thus, as it is seen from Fig. 2, a gluon radiated in the initial state (ISR) can have its own non-zero transverse momentum $P_t^{ISR} \neq 0$. It leads to the non-zero transverse momenta of partons that appear in the initial state of fundamental $2 \rightarrow 2$ QCD subprocesses (1a) and (1b). As a result of the transverse momentum conservation, a disbalance of the transverse momentum of a photon P_t^{γ} and of a parton P_t^{part} produced in the fundamental $2 \rightarrow 2$ process $5+6 \rightarrow 7+8$, shown in Figs. 2 and 3 (and thus, finally, of a jet produced by this parton), will take place.

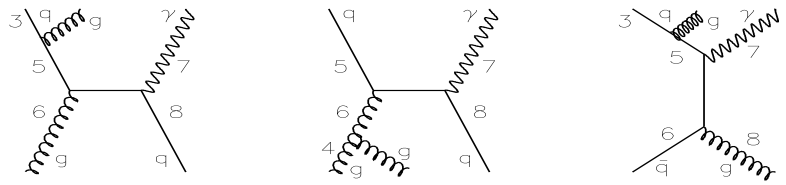

Fig. 2: Some of Feynman diagrams of direct photon production including gluon radiation in the initial state.

We shall choose the modules of a vector sum of transverse momentum vectors $\vec{P_t}^5$ and $\vec{P_t}^6$ of incoming (into $2 \rightarrow 2$ fundamental QCD subprocesses $5+6 \rightarrow 7+8$) partons, shown on lines 5 and 6 in Fig. 2, as well as the sum of their modules as two quantitative measures

$$P_t^{5+6} = |\vec{P_t}^5 + \vec{P_t}^6|, \qquad P_t 56 = |P_t^5| + |P_t^6| \tag{3}$$

to estimate the P_t disbalance caused by ISR. The modules of the vector sum

$$P_t^{\gamma+Jet} = |\vec{P_t}^{\gamma} + \vec{P_t}^{Jet}|. \tag{4}$$

will be used as an estimator of the final state P_t disbalance in the "$\gamma + Jet$" system.

The numeration notations in these Feynman diagrams as well as in formulae (3) and (4) are chosen to be in correspondence with those used in PYTHIA for describing parton–parton subprocess, displayed schematically in Fig. 3. The "ISR" block describes the initial state radiation process that can take place before the fundamental hard $2 \rightarrow 2$ process.

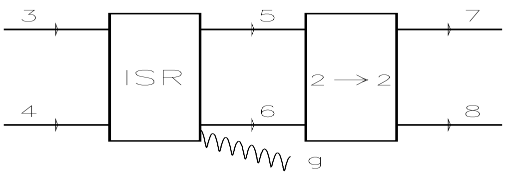

Fig. 3: PYTHIA "diagram" of $2 \rightarrow 2$ process (5+6→7+8) with a block (3+4→5+6) of initial state radiation (ISR).

2.3 Primordial parton k_T effect.

A possible non-zero value of the intrinsic parton velocity inside a colliding proton may be another source of the P_t^{γ} and P_t^{part} disbalance in the final state . Its reasonable value is supposed to lead to the value of $k_T \leq 1.0\ GeV/c$. It should be noted that sometimes in the literature the summarized effect of ISR and of the intrinsic parton transverse momentum is denoted by k_T. Here we follow the approach used in PYTHIA where these two sources of disbalance are treated separately and switched on by different keys (MSTP(61) for ISR and PARP(91), PARP(93) and MSTP(91) for k_T). Below we shall keep the value of k_T to be fixed by PYTHIA default value $\langle k_T \rangle$=0.44 GeV/c. Its possible variation influence on ${P_t}^{\gamma}$ and ${P_t}^{Jet}$ disbalance will be discussed in detail in our following paper [15]. The general conclusion from there is that any variation of k_T within reasonable boundaries (as well as beyond them) does not produce a large effect in the case when the initial state radiation is switched on. The last one gives a dominant contribution.

3. CHOICE OF MEASURABLE PHYSICAL VARIABLES FOR "$\gamma + Jet$" PROCESS AND OF CUTS FOR BACKGROUND REDUCTION.

Another than (1a) and (1b) QCD processes with large cross sections, being by orders of magnitude higher than the "$\gamma + Jet$" cross section, can also contain high P_t photons and jets in final states. So, we face the problem of signal "$\gamma + Jet$" events selection out from the large QCD background. Here we shall discuss the choice of physical variables that would be useful under some cuts on their values to select the desirable processes with direct photons ("γ^{dir}") production from the background events. The possible γ^{dir} candidate may originate from the $\pi-,\ \eta-,\ \omega-,\ K-$ meson decays or, may be, from a bremsstrahlung photon.

We suppose the ECAL size to be limited by $|\eta| \leq 2.61$ and HCAL to consist of the barrel (HB), end-cap (HE) and forward (HF) parts and to be limited by $|\eta| \leq 5.0$ (CMS geometry), where $\eta = -0.5\, ln\, (tan\, (\theta/2))$ is a pseudorapidity defined through a polar angle θ counted from the beam line. In the plane transverse to the beam line the azimuthal angle ϕ defines the directions of $\vec{P_t}^{Jet}$ and $\vec{P_t}^{\gamma}$.

3.1 Introduction of some new measurable physical observables and P_t balance equation.

In $pp \to \gamma + Jet + X$ events, we are going to study, the main physical object will be a high P_t jet, to be detected in the $|\eta| < 5$ region, and a direct photon, registered by ECAL up to $|\eta| < 2.61$. In these events there will be a set of particles mainly caused by beam remnants, i.e. by spectator partons fragmentation, that are flying in the direction of a non-instrumented forward part ($|\eta| > 5$) of the detector. Let us denote the total transverse momentum of these non-observable particles as

$$\sum_{i \in |\eta| > 5} \vec{P_t}^{i} \equiv \vec{P_t}^{\eta > 5}. \tag{5}$$

Among the particles with $|\eta| < 5$ there could be also neutrinos. Their total momentum will be denoted as

$$\sum_{i \in |\eta| < 5} \vec{P}_{t(\nu)}^{i} \equiv \vec{P}_{t(\nu)}. \tag{6}$$

The sum of transverse momenta of these two kinds of non-detectable particles will be denoted as ${P_t}^{miss}$:

$$\vec{P_t}^{miss} = \vec{P}_{t(\nu)} + \vec{P_t}^{\eta > 5}. \tag{7}$$

A high energetic jet can also contain neutrinos that may carry some part of the total jet energy needed to be estimated from simulation. From the total jet transverse momentum $\vec{Pt}^{Jet}$ we shall separate the part that can be measured in the detector, i.e. in the ECAL+HCAL and muon systems. Let us denote this part as $\vec{P_t}^{jet}$ (small "j"!). So, we shall present the total jet transverse momentum $\vec{P_t}^{Jet}$ as a sum of three parts:

1. $\vec{P}_{t(\nu)}^{Jet}$, containing the contribution of neutrinos that belong to the jet, i.e., a non-detectable part of jet P_t:

$$\vec{P}_{t(\nu)}^{Jet} = \sum_{i \in Jet} \vec{P}_{t(\nu)}^{i}. \tag{8}$$

2. $\vec{P}_{t(\mu)}^{Jet}$, containing the contribution of jet muons to $\vec{P_t}^{Jet}$. These muons can give a weak signal in the calorimeters but their energy can be measured in the muon system (in the region of $|\eta| < 2.4$ in the case of CMS geometry):

$$\vec{P}_{t(\mu)}^{Jet} = \sum_{i \in Jet} \vec{P}_{t(\mu)}^{i}. \tag{9}$$

Let us mention that due to the absence of the muon system and tracker beyond the $|\eta| < 2.4$ region, there exists a part of ${P_t}^{Jet}$ caused by muons with $|\eta| > 2.4$ denoted as $P_{t(\mu,|\eta|>2.4)}^{Jet}$. This part can be considered in some sense as an analog of $P_{t(\nu)}^{Jet}$ since the only trace of its presence would be weak MIP signals in ECAL and HCAL.

As for both points 1 and 2, let us say in advance that the estimation of the average values of the neutrino and muon contributions to ${P_t}^{Jet}$ (see Section 4 and also Tables 1–8 of Appendix) has shown that they are quite negligible: about 0.35% of $\langle {P_t}^{Jet} \rangle_{all}$ is due to neutrinos and about 0.25% of $\langle {P_t}^{Jet} \rangle_{all}$ — to muons, where all means averaging over all events including those without neutrinos in jets.

3. And finally, by means of $\vec{P_t}^{jet}$ we denote the part of $\vec{P_t}^{Jet}$ which includes all detectable particles of the jet [1], i.e.:

$$\vec{P_t}^{jet} = \vec{P}_{t(HCAL+ECAL)}^{Jet} + \vec{P}_{t(\mu)}^{Jet}, \quad |\eta^{\mu}| < 2.4 \tag{10}$$

Thus, we can write (for the general case of η values)

$$\vec{P_t}^{Jet} = \vec{P_t}^{jet} + \vec{P}_{t(\nu)}^{Jet} + \vec{P}_{t(\mu,|\eta^{\mu}|>2.4)}^{Jet} \tag{11}$$

In the case of $pp \to \gamma + Jet + X$ events the particles detected in the $|\eta| < 5$ region can originate from the fundamental subprocesses (1a) and (1b), that may be caused by LO diagrams, shown in Fig. 2 as well as by NLO diagrams (like those in Fig. 3 that include ISR) and also from the "underlying" event, of course.

As it was already mentioned in Section 2, the final states of the fundamental subprocesses (1a) and (1b) may contain additional jets due to the ISR and final state radiation (FSR) caused by the higher order QCD corrections to Feynman diagrams given in Fig. 1. To realize the calibration idea (see Section 2.1), we need "in situ" selection of events with a good balance of $\vec{P_t}^{\gamma}$ and the $\vec{P_t}^{jet}$ part, measurable in the detector. It means that to make a reasonable simulation, we need to have a selected set of events with a small $P_{t(\nu)}$ (and, thus, small

[1] We shall consider the issue of small P_t charged particles contribution into the total jet P_t while discussing the results of the full GEANT simulation (with account of the magnetic field effect) in our forthcoming papers.

${P_t}^{miss}$) as a model and we also have to find a way to select events without additional jets or with jets suppressed to the level of very small P_t mini-jets or clusters.

For any event let us separate the particles in the $|\eta| < 5$ region into a "$\gamma + Jet$" system (here "Jet" denotes the jet with the highest $P_t \geq 30\ GeV/c$) having the total transverse momentum $\vec{P_t}^{\gamma+Jet}$ (see (4)) that may be different from:

$$\vec{P_t}^{\gamma+jet} = \vec{P_t}^{\gamma} + \vec{P_t}^{jet}, \qquad (12)$$

in the case of neutrino presence in a jet, and a system of all other (O) particles in the $|\eta| < 5$ region beyond the "$\gamma + Jet$" system. The total transverse momentum of this system will be denoted as ${P_t}^O$ and it is a sum of P_t of additional mini-jets (or clusters) as well as of P_t of single hadrons, photons and leptons in the $|\eta| < 5$ region. Since neutrinos are present among these leptons, then the difference of $\vec{P}_{t(\nu)}$ and $\vec{P}_{t(\nu)}^{Jet}$ gives us the value of the transverse momentum

$$\vec{P}_{t(\nu)}^{O} = \vec{P}_{t(\nu)} - \vec{P}_{t(\nu)}^{Jet}, \ \ |\eta^{\nu}| < 5 \qquad (13)$$

carried out by neutrinos which do not belong to the jet but are contained in the $|\eta| < 5$ region.

Let us denote a part of $\vec{P_t}^{O}$, that can, in principle, be measured in the detector, by $\vec{P_t}^{out}$. Thus, $\vec{P_t}^{out}$ is a sum of P_t of other mini-jets or clusters (with ${P_t}^{clust}$ smaller than ${P_t}^{Jet}$) and of P_t of single hadrons (h), photons (γ) and electrons (e) with $|\eta| < 5$ and muons (μ) with $|\eta^{\mu}| < 2.4$. Below for simplicity these mini-jets and clusters will be called just "clusters". So, $\vec{P_t}^{out}$ is the following sum ($h,\ \gamma,\ e,\ \mu \notin$ Jet):

$$\vec{P_t}^{out} = \vec{P_t}^{clust} + \vec{P}_{t(h)}^{sing} + \vec{P}_{t(\gamma)}^{nondir} + \vec{P}_{t(e)} + \vec{P}_{t(\mu,|\eta^{\mu}|<2.4)}^{O}; \quad |\eta| < 5 \qquad (14)$$

And thus, finally, we have:

$$\vec{P_t}^{O} = \vec{P_t}^{out} + \vec{P}_{t(\nu)}^{O} + \vec{P}_{t(\mu,|\eta^{\mu}|>2.4)}^{O}. \qquad (15)$$

With these notations the conservation law for the P_t component of the whole "$\gamma + Jet$" (where γ is a direct photon) event is:

$$\vec{P_t}^{\gamma} + \vec{P_t}^{Jet} + \vec{P_t}^{O} + \vec{P_t}^{\eta>5} = 0 \qquad (16)$$

with last three terms defined correspondingly by (11), (15) and (5).

3.2 Definition of selection cuts for physical variables.

1. We select the events with one jet and one photon with

$${P_t}^{\gamma} \geq 40\ GeV/c\,; \qquad {P_t}^{Jet} \geq 30\ GeV/c. \qquad (17)$$

For most of our applications the jet is defined according to PYTHIA jetfinding algorithm LUCELL. The jet cone radius R in $\eta - \phi$ space ,counted from the jet initiator cell (ic), is taken as $R_{ic} = ((\Delta\eta)^2 + (\Delta\phi)^2)^{1/2} = 0.7$ Below we shall also use the value of the jet radius, counted from the center of gravity (gc) of the jet, i.e. R_{gc}. The comparison with UA1 jetfinding algorithm (taken from CMSJET program of fast simulation [16]) is presented in [13, 14].

2. To suppress the background processes, only the events with "isolated" photons are taken. To do this, we restrict:

a) the value of the scalar sum of P_t of hadrons and other particles surrounding a photon within a cone of $R^{\gamma}_{isol} = ((\Delta\eta)^2 + (\Delta\phi)^2)^{1/2} = 0.7$ ("absolute isolation cut")

$$\sum_{i \in R} {P_t}^i \equiv {P_t}^{isol} \leq P^{isol}_{tCUT}; \tag{18}$$

b) the value of a fraction ("relative isolation cut")

$$\sum_{i \in R} {P_t}^i / {P_t}^{\gamma} \equiv \epsilon^{\gamma} \leq \epsilon^{\gamma}_{CUT}; \tag{19}$$

c) we accept only the events having no charged tracks (particles) with $P_t > 1\ GeV/c$ within R^{γ}_{isol} cone around the photon candidate.

3. To be consistent with the application condition of the NLO formulae, one should avoid an infrared dangerous region and take care of P_t population in the region close to a photon (see [21-23]). In accordance with [22] we also restrict the scalar sum of P_t of particles around a photon within a cone of a smaller radius $R_{singl} = 0.175 = 1/4\, R^{\gamma}_{isol}$.

Due to this cut,

$$\sum_{i \in R_{singl}} {P_t}^i \equiv {P_t}^{singl} \leq 2\ GeV/c, \qquad (i \neq\ \gamma - dir). \tag{20}$$

an "isolated" photon with high P_t also becomes a "single" one within an area of 8 towers (of 0.087x0.087 size according to CMS geometry) which surround the tower hitted by it (analog of 3×3 tower window algorithm).

4. We also consider the structure of every event with the photon candidate at a more precise level of 5x5 crystal cells window (size of one CMS HCAL tower) with a cell size of 0.0175x0.0175. To suppress the background events with photons resulting from high energetic π^0-, $\eta-$, $\omega-$ and K^0_S- mesons,we apply in addition the following cut:

a) the ECAL signal can be considered as a candidate to be a direct photon if it fits inside the 3x3 ECAL crystal cell window with the highest P_t γ/e in the center;

b) the value of a scalar sum of P_t (${P_t}^{sum}$) of stable particles in the 5x5 crystal cell window in the region out of a smaller 3x3 crystal cell window (typical size of photon shower in ECAL found from GEANT simulation with CMSIM package), having the cell with the direct photon candidate (the largest P_t γ/e) as the central one, should be restricted by $1\, GeV/c$, i.e.

$${P_t}^{sum} \leq 1\ GeV/c; \tag{21}$$

c) we require the absence of a high P_t hadron in this 5x5 crystal cell window (that means an imposing of an upper cut on the HCAL signal at least in the one-tower area) around the direct photon:

$${P_t}^{hadr} \leq 5\ GeV/c. \tag{22}$$

We can not reduce this value to, for example, 2-3 GeV/c, because a hadron with P_t below 2-3 GeV/c deposits most of its energy in ECAL and may not reveal itself in HCAL.

5. We select the events with the vector $\vec{P_t}^{Jet}$ being "back-to-back" to the vector $\vec{P_t}^{\gamma}$ (in the plane transverse to the beam line) within $\Delta\phi$ defined by equation:

$$\phi_{(\gamma,jet)} = 180^\circ \pm \Delta\phi \quad (\Delta\phi = 15^\circ, 10^\circ, 5^\circ) \tag{23}$$

(5° is a size of one CMS HCAL tower in ϕ) for the following definition of the angle $\phi_{(\gamma,jet)}$

$$\vec{P_t}^{\gamma}\vec{P_t}^{Jet} = {P_t}^{\gamma}{P_t}^{Jet} \cdot cos(\phi_{(\gamma,jet)}), \quad \text{with } {P_t}^{\gamma} = |\vec{P_t}^{\gamma}|, \ {P_t}^{Jet} = |\vec{P_t}^{Jet}|.$$

6. The initial state radiation (ISR) manifests itself as some final state cluster or mini-jet activity. To suppress it, we impose a new cut condition that was not used earlier in previous experiments: we choose the events that do not have any other jet-like or cluster high P_t activity, i.e. ${P_t}^{clust}$ (taking the cluster cone $R_{clust}(\eta,\phi) = 0.7$), being higher than some threshold P_{tCUT}^{clust} value, i.e. we select the events with

$${P_t}^{clust} \le P_{tCUT}^{clust}, \tag{24}$$

where clusters are found by one and the same jetfinder used to find the jet in the event.

7. We limit the value of modulus of the vector sum of $\vec{P_t}$ of all particles, except those in the "$\gamma + Jet$" system, that fit into the region covered by ECAL and HCAL (i.e. the cells "beyond the jet and photon" regions):

$$\left| \sum_{i \notin Jet, \gamma-dir} \vec{P_t}^{i} \right| \equiv {P_t}^{out} \le P_{tCUT}^{out}, \ \ |\eta| < 5 \tag{25}$$

The importance of P_{tCUT}^{out} and P_{tCUT}^{clust} parameters to reduce the background will be demonstrated in the forthcoming papers [13–15].

Below the selection cuts 1 – 7 will be referred as "Selection 1". The last two of them, 6 and 7, are new criteria, not used in previous experiments. In addition to them one more new object, named an "isolated jet", will be introduced.

8. To do this we also involve a new requirement of "jet isolation", i.e. the presence of a "clean enough" (in the sense of limited P_t activity) region inside the ring (of $\Delta R = 0.3$ size) around the jet. Following this picture we restrict the value of the ratio of the scalar sum of transverse momenta of particles belonging to this ring, i.e.

$${P_t}^{ring}/{P_t}^{\gamma} \equiv \epsilon^{jet} \le 2\%, \quad \text{where} \quad {P_t}^{ring} = \sum_{i \in 0.7 < R < 1} |\vec{P_t}^{i}|. \tag{26}$$

The set of events that pass under the cuts 1 – 8 will be called as "Selection 2".

9. In the following "Selection 3" we shall keep only those events in which one and the same jet (i.e. up to good accuracy having the same values of ${P_t}^{Jet}$, R^{jet} and $\Delta\phi$) is found simultaneously by every of two jetfinders used here: UA1 and LUCELL. For these jets (and also clusters) we require the following conditions:

$${P_t}^{Jet} > 30\,GeV/c, \qquad {P_t}^{clust} < P_{tCUT}^{clust}, \qquad \Delta\phi < 15^\circ (10^\circ,\ 5^\circ), \qquad \epsilon^{jet} \le 2\% \tag{27}$$

The exact values of cut parameters, i.e. P_{tCUT}^{isol}, ϵ_{CUT}^{γ}, ϵ^{jet}, P_{tCUT}^{clust}, P_{tCUT}^{out}, will be specified below, since they may be different, for instance, for various ${P_t}^{\gamma}$-intervals (being more loose for higher ${P_t}^{\gamma}$).

10. As we have already mentioned in Section 3.1, one can expect reasonable results of the calibration procedure modeling only by using a set of selected events with a small value of ${P_t}^{miss}$. So, we also use the following cut:

$$ {P_t}^{miss} \le P_{tCUT}^{miss}. \tag{28} $$

Due to this reason in Section 4, we shall study the influence of ${P_t}^{miss}$ parameter on the selection of events with a reduced value of $P_{t(\nu)}^{Jet}$. The aim of the event selection with a small value of $P_{t(\nu)}^{Jet}$ is quite obvious: we need a set of events with a reduced value of ${P_t}^{Jet}$ uncertainty due to possible presence of a non-detectable neutrino contribution to a jet.

To conclude this section, let us rewrite the basic P_t-balance equation (16) of the previous section by means of notations introduced here in the form more suitable to present results in further papers [12–15]. For this purpose we shall rewrite equation (16) in the following scalar form:

$$ \frac{{P_t}^{\gamma} - {P_t}^{Jet}}{{P_t}^{\gamma}} = (1 - cos\Delta\phi) + P_t(O + \eta > 5)/{P_t}^{\gamma}, \tag{29} $$

where $P_t(O+\eta>5) \equiv (\vec{P_t}^{O} + \vec{P_t}^{|\eta|>5)}) \cdot \vec{n}^{Jet}$ with $\vec{n}^{Jet} = \vec{P_t}^{Jet}/{P_t}^{Jet}$.

As it will be shown in [12–14], the first term in the right-hand part of the equation (29) is negligibly small and tends to decrease more with a growth of the energy. So, the main source of the P_t disbalance in the "$\gamma + Jet$" system is a term $P_t(O+\eta>5)/{P_t}^{\gamma}$.

4. ESTIMATION OF NON-DETECTABLE PART OF ${P_t}^{Jet}$

In Section 3.1 we have separated the transverse momentum of the jet, i.e. ${P_t}^{Jet}$, into two parts: a detectable one ${P_t}^{jet}$ and a non-measurable part, consisting of $P_{t(\nu)}^{Jet}$ (see (8)) and $P_{t(\mu,|\eta|>2.4)}^{Jet}$ (see (11)) [2]. In the same way we have done analogous separation according to equation (15) of the transverse momentum of other particles, i.e. ${P_t}^{O}$, excluding direct photon (or candidate to be detected as a direct photon), into detectable part ${P_t}^{out}$ and non-measurable part consisting of $P_{t(\nu)}^{O}$ (see (13)) and $P_{t(\mu,|\eta|>2.4)}^{O}$ (see (15)).

Here we present an estimation of averaged values of transverse momenta of the total ${P_t}^{Jet}$ carried out by non-detectable particles. For this aim we use a bank of the signal "$\gamma + Jet$" events generated for three intervals of ${P_t}^{\gamma}$ with the restrictions (17) – (24) and the following cuts are fixed as follows:

$$ P_{tCUT}^{isol} = 20\, GeV/c, \;\; \epsilon_{CUT}^{\gamma} = 15\%, \;\; \Delta\phi = 15^{\circ}, \;\; P_{tCUT}^{clust} = 30\, GeV/c. \tag{30} $$

No restriction for the ${P_t}^{out}$ value was done. The results of analysis of these events are presented in Figs. 4 and 5.

The first row of Fig. 4 contains ${P_t}^{miss}$ spectra in the "$\gamma + Jet$" events for different ${P_t}^{\gamma}$ intervals. Their practical independence (up to the good accuracy) on ${P_t}^{\gamma}$ is clearly seen.

In the second row of Fig. 4 we present the spectra of ${P_t}^{miss}$ for the events (denoted as $P_{t(\nu)}^{Jet} > 0$) having a non-zero $P_{t(\nu)}^{Jet}$ component in ${P_t}^{Jet}$. For these figures the ${P_t}^{miss}$ spectrum dependence on the direct photon ${P_t}^{\gamma}$ (that is equal, approximately, to ${P_t}^{Jet}$) is seen.

[2] Firstly we shall consider the case of switched off decays of $\pi^{\pm}$ and $K^{\pm}$ mesons (according to the PYTHIA default agreement, $\pi^{\pm}$ and $K^{\pm}$ mesons are stable).

So, the spectra tails as well as the mean values are shifting to a large ${P_t}^{miss}$ region with ${P_t}^{Jet}$ growth. At the same time a peak position remains in the region of ${P_t}^{miss} < 5\ GeV/c$. From the comparison of the number of entries in the second row plots of Fig. 4 with those in the first row it can be concluded that the part of events with the jet having the non-zero neutrinos contribution (${P_t}^{Jet}_{(\nu)} > 0$) has the same size of about 3.3% in all ${P_t}^{\gamma}$ intervals.

The same spectra of ${P_t}^{miss}$ for events with ${P_t}^{Jet}_{(\nu)} > 0$ show what amount of these events would remain after imposing a cut on ${P_t}^{miss}$ in every ${P_t}^{\gamma}$ interval. The important thing here is that the reduction of the number of events with ${P_t}^{Jet}_{(\nu)} > 0$ in every ${P_t}^{\gamma}$ interval leads to reducing the mean value of ${P_t}^{Jet}_{(\nu)}$, i.e. a value averaged over all collected events. This value, found from PYTHIA generation, serves as a model correction Δ_ν and it has to be estimated for the proper determination of the total ${P_t}^{Jet}$ from the measurable part ${P_t}^{jet}$: ${P_t}^{Jet} = {P_t}^{jet} + \Delta_\nu$, where $\Delta_\nu = \langle {P_t}^{Jet}_{(\nu)} \rangle_{all\ events}$.

The effect of general ${P_t}^{miss}_{CUT}$ imposing in each event of our sample is shown in the third row of Fig. 4. The upper cut ${P_t}^{miss}_{CUT} = 1000\ GeV/c$, as it is seen from the second row pictures, means the absence of any upper limit on ${P_t}^{Jet}_{(\nu)}$. The most important information that the value of the neutrinos P_t inside the jet, being averaged over all events, can reach the value of ${P_t}^{Jet}_{(\nu)} \approx 1\ GeV/c$ at ${P_t}^{\gamma} \geq 300\ GeV/c$ comes from the right-hand plot of the third row in Fig. 4. From the comparison of the plots from the second row with the corresponding plots [3] from the third row we see that the first cut ${P_t}^{miss}_{CUT} = 20\ GeV/c$ for the first $40 < {P_t}^{\gamma} < 50\ GeV/c$ interval reduces the number of entries by less than 0.5% and the mean value of ${P_t}^{Jet}_{(\nu)}$ — by less than 10%. A more restrictive cut ${P_t}^{miss}_{CUT} = 5\ GeV/c$ reduces the value of $\langle {P_t}^{Jet}_{(\nu)} \rangle$ by three times and leads to approximate twofold drop of the number of events.

From these Figures we see that for the interval $300 < {P_t}^{\gamma} < 360$ the number of events with jets including neutrino (second row) is about 3.3% (Entries=3001) of the total number of the generated "$\gamma + Jet$" events (Entries=89986). A very restrictive ${P_t}^{miss}_{CUT}$=5 GeV/c cut leads to the reduction factor for $\langle {P_t}^{Jet}_{(\nu)} \rangle$ of about 50. As it is seen from the plot in the bottom right-hand corner of Fig. 4, the ${P_t}^{Jet}_{(\nu)}$ spectrum for the remaining events (Entries=57475) finishes at ${P_t}^{Jet}_{(\nu)} = 10\ GeV/c$ and sharply peaks at ${P_t}^{Jet}_{(\nu)} = 0$. The averaged value of ${P_t}^{Jet}_{(\nu)}$ under this peak is equal to 0.022 GeV/c. So, with this cut on ${P_t}^{miss}$ the neutrinos give a negligible contribution to ${P_t}^{Jet}$.

At the same time we see that application of the moderate cut ${P_t}^{miss}_{CUT} = 10\ GeV/c$ for $300 < {P_t}^{Jet} < 360\ GeV/c$ interval strongly reduces (by 20 times) the mean value of ${P_t}^{Jet}_{(\nu)}$ (from $1\ GeV/c$ down to $< {P_t}^{Jet}_{(\nu)} >= 0.05\ GeV/c$) at about 10% reduction of the total number of events in this ${P_t}^{Jet}$ (or ${P_t}^{\gamma}$) interval.

In the case of $100 < {P_t}^{Jet} < 120\ GeV/c$ interval, as we see from the third row of Fig. 4, the same cut ${P_t}^{miss}_{CUT} = 10\ GeV/c$ reduces the mean value of ${P_t}^{Jet}_{(\nu)}$ by 5 times (from $0.5\ GeV/c$ down to $< {P_t}^{Jet}_{(\nu)} >= 0.09\ GeV/c$) with the same 10% reduction of the total number of events.

It should be noted that in the less dangerous (from the point of view of the size of

[3] That includes the values of ${P_t}^{miss}_{CUT}$ and the corresponding number of entries remained after ${P_t}^{miss}_{CUT}$ imposing as well as the mean value of ${P_t}^{Jet}_{(\nu)}$, denoted as "Mean" (being equal to an averaged $\langle {P_t}^{Jet}_{(\nu)} \rangle$ value over the number of the remained entries.

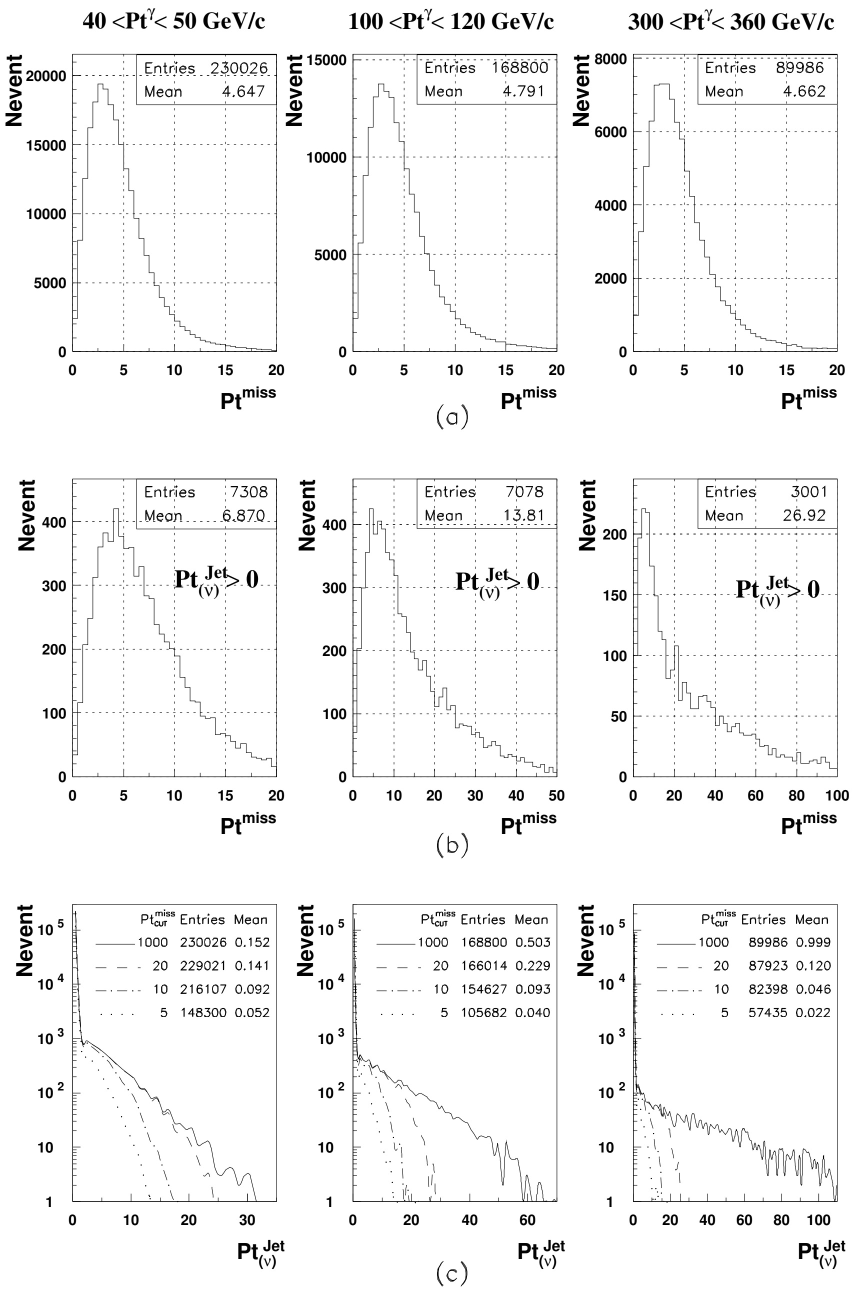

Fig. 4: a) ${P_t}^{miss}$ spectra in all events; b) ${P_t}^{miss}$ spectra in events having jets with non-zero P_t neutrinos, i.e. ${P_t}_{(\nu)}^{Jet} > 0$; c) ${P_t}_{(\nu)}^{Jet}$ spectra behavior for different values of ${P_t}_{CUT}^{miss}$ values in various ${P_t}^{Jet}(\approx {P_t}^{\gamma})$ intervals.

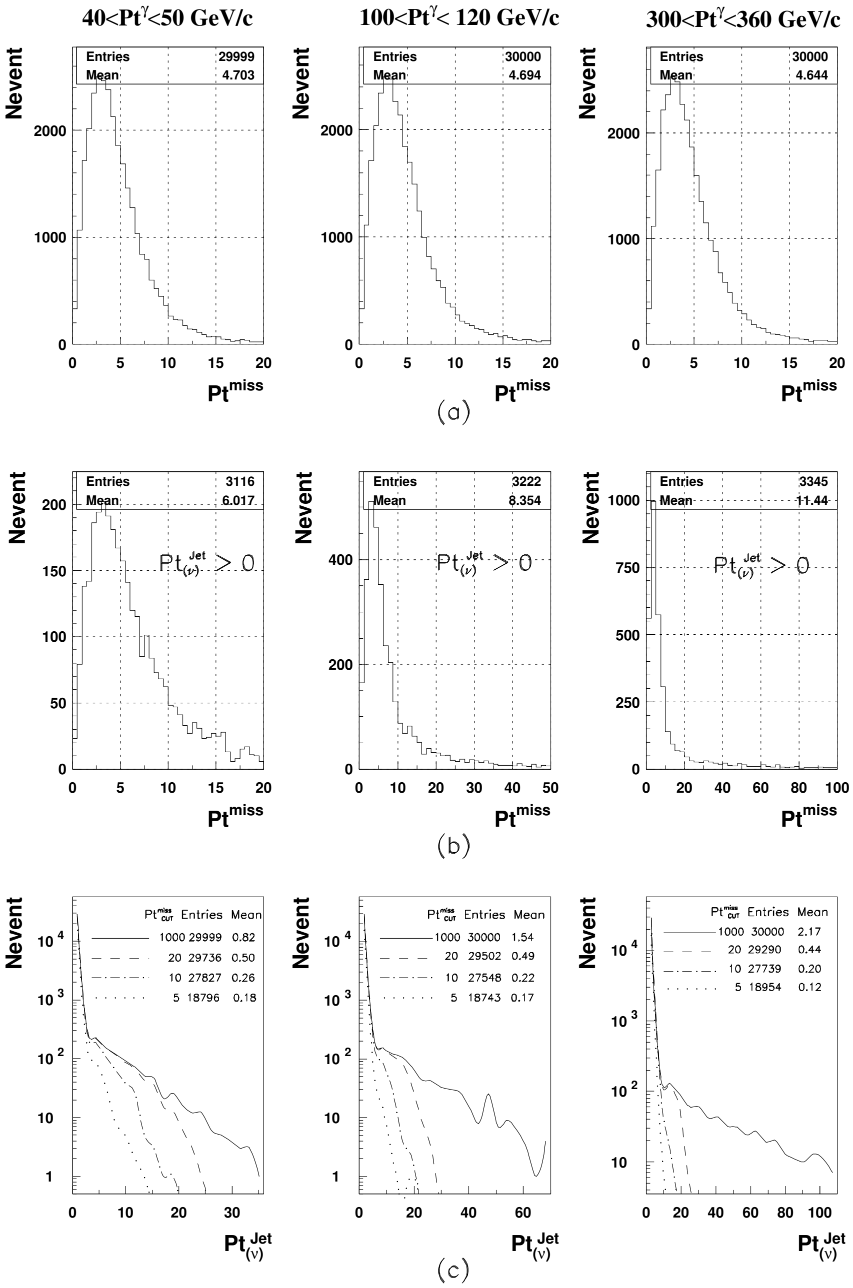

Fig. 5: a) ${P_t}^{miss}$ spectra in all events; b) ${P_t}^{miss}$ spectra in events having jets with non-zero P_t neutrinos, i.e. $P_{t}{}_{(\nu)}^{Jet} > 0$; c) $P_{t}{}_{(\nu)}^{Jet}$ spectra behavior for different values of $P_{t}{}_{CUT}^{miss}$ values in various ${P_t}^{Jet}(\approx {P_t}^{\gamma})$ intervals. $K^{\pm}-$decays are allowed inside the solenoid of $R = 129\ cm$ and $L = 317\ cm$.

neutrino P_t content in a jet) $40 < {P_t}^{Jet} < 50\ GeV/c$ interval we have already a very small mean value of $P_{t(\nu)}^{Jet}$ equal to $0.152\ GeV/c$ without imposing any P_{tCUT}^{miss}.

The analogous (to neutrino) situation holds for $P_{t(\mu)}^{Jet}$ contribution.

The detailed information about the values of non-detectable $P_{t(\nu)}^{Jet}$, averaged over all events (no cut on ${P_t}^{miss}$ was used), as well as about mean values of muons P_t from jet $P_{t(\mu)}^{Jet}$, is presented in Tables 1–8 of Appendix for the sample of events with jets which are completely contained in the barrel region of HCAL ($|\eta^{jet}| < 1.4$, "HB-events", see [12]). In these tables the ratio of the number of events with non-zero $P_{t(\nu)}^{Jet}$ to the total number of events is denoted by $R_{event}^{\nu\in Jet}$ and the ratio of the number of events with non-zero $P_{t(\mu)}^{Jet}$ to the total number of events is denoted by $R_{event}^{\mu\in Jet}$. The ${P_t}^{miss}$ quantity in events with $P_{t(\nu)}^{Jet} > 0$ is denoted in these tables as $P_{t\nu\in Jet}^{miss}$ and is given there for four ${P_t}^{\gamma}$ intervals and other P_{tCUT}^{clust} values than in the second row plots of Figs. 4 and 5. From Tables 1–8 we see that the averaged of ${P_t}^{miss}$ value being calculated by using of only the events with $P_{t(\nu)}^{Jet} > 0$, i.e. $\langle P_{t\nu\in Jet}^{miss}\rangle$, is about 7 GeV/c for $40 < {P_t}^{\gamma} < 50\ GeV/c$ interval. It increases to about 32 GeV/c for $300 < {P_t}^{\gamma} < 360\ GeV/c$. It should be noted that the averaged values of the modulus of $P_{t(\nu)}^{Jet}$ (see formula (8)) presented in the second and third lines of Tables 1–6 from the Appendix, coincide with the averaged values of Δ_ν up to the three digits due to practical collinearity of $\vec{P}_t^{\ Jet}$ and $\vec{P}_t^{\ jet}$ vectors, i.e. $<P_{t(\nu)}^{Jet}>=<\Delta_\nu>$.

Tables 1–8 contain the lines with an additional information on the numbers of the "$\gamma+Jet$" events with the jets produced by $c-$ and $b-$ quarks, i.e. $Nevent_{(c)}$ and $Nevent_{(b)}$, given for the integrated luminosity $L_{int} = 3\ fb^{-1}$, respectively. There are also lines that show a ratio ("$29sub/all$") of the number of the events caused by gluonic ("Compton-like") subprocess (1a) to the number of events due to the sum of (1a) and (1b) subprocesses.

Below follows the line containing the averaged values of the jet radius $<R_{jet}>$.

The value of the difference of the jet measurable part transverse momentum ${P_t}^{jet}$ and of the total jet ${P_t}^{Jet}$, averaged over all events, i.e. $\langle {P_t}^{Jet} - {P_t}^{jet}\rangle$, is presented in second lines of Tables 1–8 of Appendix in GeV/c units. This value has a sense of correction Δ_ν that should be applied to ${P_t}^{jet}$ in order to take into account P_t carried off by non-detectable particles.

It was already mentioned in Introduction that we are planning to carry out a more detailed analysis basing on GEANT package and taking into account weak decays of $\pi^\pm$ and $K^\pm$ mesons. To have an idea what changes can be expected, we shall consider only the case of allowed $K^\pm$ decays (as the main source of neutrinos and muons). The averaged values of $P_{t(\nu)}^{Jet}$ for different ${P_t}^{\gamma}$-intervals with switched on $K^\pm$ decays are given in Fig. 5 with the same meaning of all notations. Here $K^\pm$ decays are allowed inside the solenoid volume with the barrel radius $R_B = 129\ cm$ and the distance from the interaction vertex to End-cap along Z-axis $L = 317\ cm$ (CMS geometry).

From this Figure we see that in the case of allowed $K^\pm$ decays, the ${P_t}^{miss}$ spectrum for all events (compare the first rows in Fig. 4 and Fig. 5) practically does not change with ${P_t}^{Jet}(\approx {P_t}^{\gamma})$ as well as the mean value of ${P_t}^{miss}$. At the same time the ${P_t}^{miss}$ spectra change for events that contain neutrinos in the jet (second row of Fig. 5) quite noticeably. It should be noted that the amount of such events grows up to 10% as compared with 3% in the case considered in Fig. 4, but the mean values of ${P_t}^{miss}$ do not grow so strongly with ${P_t}^{\gamma}$ as it was seen in Fig. 4. The mean value of ${P_t}^{miss}$ changes only twice from $6.0\ GeV/c$ for the interval $40 < {P_t}^{\gamma} < 50$ to $11.4\ GeV/c$ for the interval $300 < {P_t}^{\gamma} < 360$. Now we compare the third row pictures in Figs. 4 and 5. We see that the mean value of $P_{t(\nu)}^{Jet}$, carried out by neutrinos of the jet grows up from the value of about $\langle P_{t(\nu)}^{Jet}\rangle \approx 0.8\ GeV/c$ at $40 < {P_t}^{\gamma} < 50\ GeV/c$ to the value of $\langle P_{t(\nu)}^{Jet}\rangle \approx 2.2\ GeV/c$ at $300 < {P_t}^{\gamma} < 360\ GeV/c$, i.e. it changes as $2\% \to 0.7\%$ of ${P_t}^{Jet}$. From the same pictures of Fig. 5 we see that the general cut $P_{tCUT}^{miss} = 20\ GeV/c$ would reduce the contribution of neutrinos into ${P_t}^{Jet}$ to the value $\langle P_{t(\nu)}^{Jet}\rangle \approx 0.5\ GeV/c$ in all ${P_t}^{Jet}$ intervals, while the cut $P_{tCUT}^{miss} = 10\ GeV/c$ would lead to the value of $\langle P_{t(\nu)}^{Jet}\rangle \approx 0.20 - 0.26\ GeV/c$. (that is quite acceptable) with $\approx 9\%$ reduction of the event number.

5. SUMMARY

The possibility of the jet energy scale setting and hadron calorimeter calibration at LHC energies by using the "$\gamma + Jet$" process is considered for the case of low luminosity ($10^{33}\ cm^2 s^{-1}$).

The initial state radiation (ISR) as the main source of the P_t disbalance in the "$\gamma + Jet$" system is discussed. New variables that enter the P_t-balance equation are considered. The new cuts (see Section 3) P_{tCUT}^{out} and P_{tCUT}^{clust} (in addition to the cut on $\phi_{(\gamma,jet)}$ angle used previously in other experiments) as well as a new object of "isolated jet" are introduced here. The consequences of their variation and the choice of their most preferable values to select the events with a good ${P_t}^{\gamma}$ and ${P_t}^{jet}$ balance will be discussed in [12–15].

The values of the non-detectable part of ${P_t}^{Jet}$ caused by neutrinos are estimated for different ${P_t}^{Jet}$ intervals. It is found that ${P_t}^{\gamma}$ and ${P_t}^{Jet}$ balance can be influenced by neutrino energy leakage from the jet. The $P_{tCUT}^{miss} = 10\ GeV/c$ is proved to be sufficient for reducing the jet energy leakage caused by neutrinos to an acceptable level with about of 9% loss of events.

After the detailed study of neutrinos and muons contribution to ${P_t}^{Jet}$ done here, the following papers will be concentrated on the contribution of hadrons, photons and electrons.

We would like to emphasize once more that the values of selection cuts, given here, are not a dogma for us. Our aim is to present an estimation of a number of events that can be selected in some unit of time chosen here as one month of LHC continuous operation (i.e. $3000\, pb^{-1} = 3\, fb^{-1}$). In future calibration "in situ" one can collect these "$\gamma + Jet$" events and in parallel classify them according to different Selection criteria (1, 2 and 3; see Section 3.2) for increasing the degree of accuracy.

6. ACKNOWLEDGMENTS

We are greatly thankful to D. Denegri for having offered this theme to study, fruitful discussions and permanent support and encouragement. It is a pleasure for us to express our recognition for helpful discussions to P. Aurenche, M. Dittmar, M. Fontannaz, J.Ph. Guillet, M.L. Mangano, E. Pilon, H. Rohringer, S. Tapprogge and especially to J. Womersley for supplying us with the preliminary version of paper [1].

References

[1] D0 Collaboration, F. Abachi *et al.*, NIM **A424** (1999)352.

[2] CDF Collaboration. F. Abe *et al.*, Phys.Rev. **D50** (1994)2966; F. Abe *et al.*, Phys.Rev.Lett. **73** (1994)225.

[3] D. Denegri, R. Kinnunen, A. Nikitenko, CMS Note 1997/039 "Study of calorimeter calibration with τ's in CMS".

[4] R. Kinnunen, A. Nikitenko, CMS Note 1997/097 "Study of calorimeter calibration with pions from jets in CMS".

[5] J. Womersley. A talk at CMS Week meeting, Aachen, 1997.

[6] J. Freeman, W. Wu, **draft** "In situ calibration of CMS HCAL calorimeter".

[7] R. Mehdiyev, I. Vichou, ATLAS Note ATL-COM-PHYS-99-054 (1999) "Hadronic jet energy scale calibration using Z+jet events".

[8] ATLAS Detector and Physics Performance, Technical Design Report, Volumes **1, 2**, 1999. CERN/LHCC 99-14.

[9] N.B. Skachkov, V.F. Konoplyanikov D.V. Bandourin, "Photon – jet events for calibration of HCAL". Second Annual RDMS CMS Collaboration Meeting. CMS-Document, 1996–213. CERN, December 16-17, 1996, p.7-23.

[10] N.B. Skachkov, V.F. Konoplyanikov D.V. Bandourin, "γ-direct + 1 jet events for HCAL calibration". Third Annual RDMS CMS Collaboration Meeting. CMS-Document, 1997–168. CERN, December 16-17, 1997, p.139-153.

[11] T. Sjostrand, Comp.Phys.Comm. **82** (1994)74.

[12] D.V. Bandourin, V.F. Konoplyanikov, N.B. Skachkov. "Jet energy scale setting with "$\gamma + Jet$" events at LHC energies. Event rates, P_t structure of jet". JINR Communication, JINR, Dubna, 2000-

[13] D.V. Bandourin, V.F. Konoplyanikov, N.B. Skachkov. "Jet energy scale setting with "$\gamma + Jet$" events at LHC energies. Minijets and cluster suppression and ${P_t}^{\gamma} - {P_t}^{Jet}$ disbalance". JINR Communication, JINR, Dubna, 2000-

[14] D.V. Bandourin, V.F. Konoplyanikov, N.B. Skachkov. "Jet energy scale setting with "$\gamma + Jet$" events at LHC energies. Selection of events with a clean "$\gamma + Jet$" topology and ${P_t}^{\gamma} - {P_t}^{Jet}$ disbalance.". JINR Communication, JINR, Dubna, 2000-

[15] D.V. Bandourin, V.F. Konoplyanikov, N.B. Skachkov. "Jet energy scale setting with "$\gamma + Jet$" events at LHC energies. Detailed study of the background suppression". JINR Communication, JINR, Dubna, 2000-

[16] S. Abdullin, A. Khanov, N. Stepanov, CMS Note CMS TN/94–180 "CMSJET".

[17] S. Frixione, Phys.Lett. **B429** (1998)369.

[18] S. Catani, M. Fontannaz and E. Pilon, Phys.Rev. **D58** (1998)094025

APPENDIX

$$40 < P_t^{\gamma} < 50\ GeV/c$$

Table 1: Selection 1. $\phi_{(\gamma,jet)} = 180^\circ \pm 15^\circ$. UA1 algorithm. $L_{int} = 3\ fb^{-1}$

Pt^{clust}_{CUT}	30	20	15	10	5
Pt^{jet}	43.021	42.771	42.679	42.755	43.202
Pt^{Jet}–Pt^{jet}	0.168	0.167	0.161	0.160	0.127
$Pt^{Jet}_{(\nu)}$	0.169	0.168	0.162	0.161	0.128
$R^{\nu\in Jet}_{event}$	0.033	0.033	0.033	0.033	0.027
$Pt^{Jet}_{(\mu)}$	0.100	0.099	0.096	0.099	0.087
$R^{\mu\in Jet}_{event}$	0.018	0.018	0.017	0.017	0.014
Pt^{miss}	4.551	4.511	4.470	4.399	4.134
$Pt^{miss}_{\nu\in Jet}$	7.054	6.942	6.843	6.777	6.576
Nevent$_{(c)}$	312191	287694	253628	180811	40334
Nevent$_{(b)}$	40098	36223	30495	20689	3639
$29sub/all$	0.92	0.91	0.91	0.91	0.90
R_{jet}	0.60	0.60	0.60	0.60	0.59
Entries	56532	52588	46991	34426	8421

Table 2: Selection 1. $\phi_{(\gamma,jet)} = 180^\circ \pm 15^\circ$. LUCELL algorithm. $L_{int} = 3\ fb^{-1}$

Pt^{clust}_{CUT}	30	20	15	10	5
Pt^{jet}	43.253	43.000	42.949	43.026	43.408
Pt^{Jet}–Pt^{jet}	0.168	0.165	0.160	0.156	0.121
$Pt^{Jet}_{(\nu)}$	0.169	0.166	0.161	0.157	0.121
$R^{\nu\in Jet}_{event}$	0.033	0.033	0.033	0.032	0.027
$Pt^{Jet}_{(\mu)}$	0.103	0.100	0.098	0.093	0.094
$R^{\mu\in Jet}_{event}$	0.018	0.018	0.017	0.017	0.015
Pt^{miss}	4.556	4.510	4.474	4.382	4.104
$Pt^{miss}_{\nu\in Jet}$	7.027	6.915	6.834	6.745	6.595
Nevent$_{(c)}$	304172	277451	241228	164132	36021
Nevent$_{(b)}$	39256	34740	29248	18937	3167
$29sub/all$	0.92	0.91	0.91	0.90	0.90
R_{jet}	0.65	0.65	0.65	0.64	0.63
Entries	54922	50723	44738	31455	7751

$$100 < P_t^{\gamma} < 120\ GeV/c$$

Table 3: Selection 1. $\phi_{(\gamma,jet)} = 180° \pm 15°$. UA1 algorithm. $L_{int} = 3\ fb^{-1}$

Pt^{clust}_{CUT}	30	20	15	10	5
Pt^{jet}	102.627	104.675	105.575	106.329	106.917
Pt^{Jet}–Pt^{jet}	0.546	0.538	0.523	0.501	0.488
$Pt^{Jet}_{(\nu)}$	0.548	0.539	0.525	0.502	0.489
$R^{\nu\in Jet}_{event}$	0.044	0.042	0.040	0.038	0.034
$Pt^{Jet}_{(\mu)}$	0.258	0.249	0.234	0.228	0.216
$R^{\mu\in Jet}_{event}$	0.023	0.022	0.021	0.019	0.019
Pt^{miss}	5.166	5.139	5.102	5.053	4.913
$Pt^{miss}_{\nu\in Jet}$	14.245	14.512	14.817	14.831	15.412
Nevent$_{(c)}$	18289	13417	10124	6149	1051
Nevent$_{(b)}$	2887	1989	1435	779	113
$29sub/all$	0.89	0.89	0.88	0.88	0.86
R_{jet}	0.61	0.61	0.61	0.61	0.60
Entries	63316	48178	37512	23472	4467

Table 4: Selection 1. $\phi_{(\gamma,jet)} = 180° \pm 15°$. LUCELL algorithm. $L_{int} = 3\ fb^{-1}$

Pt^{clust}_{CUT}	30	20	15	10	5
Pt^{jet}	103.378	105.266	106.137	106.938	107.216
Pt^{Jet}–Pt^{jet}	0.549	0.544	0.524	0.475	0.491
$Pt^{Jet}_{(\nu)}$	0.552	0.546	0.525	0.477	0.492
$R^{\nu\in Jet}_{event}$	0.045	0.043	0.041	0.037	0.034
$Pt^{Jet}_{(\mu)}$	0.260	0.249	0.240	0.223	0.198
$R^{\mu\in Jet}_{event}$	0.023	0.022	0.021	0.019	0.017
Pt^{miss}	5.168	5.136	5.110	5.010	4.897
$Pt^{miss}_{\nu\in Jet}$	14.169	14.506	14.527	14.442	15.832
Nevent$_{(c)}$	17309	12498	9257	5137	984
Nevent$_{(b)}$	2704	1866	1308	620	102
$29sub/all$	0.89	0.89	0.88	0.87	0.85
R_{jet}	0.65	0.65	0.65	0.65	0.64
Entries	59683	44691	34139	20072	4019

$$200 < P_t^{\gamma} < 240 \; GeV/c$$

Table 5: Selection 1. $\phi_{(\gamma,jet)} = 180° \pm 15°$. UA1 algorithm. $L_{int} = 3\ fb^{-1}$

Pt^{clust}_{CUT}	30	20	15	10	5
Pt^{jet}	211.973	213.370	214.124	214.874	215.511
$Pt^{Jet}{-}Pt^{jet}$	0.886	0.874	0.823	0.768	0.639
$Pt^{Jet}_{(\nu)}$	0.889	0.877	0.825	0.770	0.640
$R^{\nu\in Jet}_{event}$	0.039	0.038	0.037	0.035	0.033
$Pt^{Jet}_{(\mu)}$	0.420	0.399	0.360	0.338	0.344
$R^{\mu\in Jet}_{event}$	0.020	0.019	0.019	0.017	0.016
Pt^{miss}	5.558	5.529	5.444	5.368	5.130
$Pt^{miss}_{\nu\in Jet}$	24.382	24.517	23.705	23.182	20.955
Nevent$_{(c)}$	1081	753	547	317	52
Nevent$_{(b)}$	152	100	70	36	6
$29sub/all$	0.86	0.85	0.85	0.84	0.82
R_{jet}	0.62	0.62	0.62	0.62	0.61
Entries	52542	37741	28477	17189	3142

Table 6: Selection 1. $\phi_{(\gamma,jet)} = 180° \pm 15°$. LUCELL algorithm. $L_{int} = 3\ fb^{-1}$

Pt^{clust}_{CUT}	30	20	15	10	5
Pt^{jet}	212.521	213.982	214.736	215.460	216.044
$Pt^{Jet}{-}Pt^{jet}$	0.866	0.850	0.802	0.742	0.568
$Pt^{Jet}_{(\nu)}$	0.869	0.853	0.805	0.744	0.569
$R^{\nu\in Jet}_{event}$	0.038	0.037	0.036	0.034	0.028
$Pt^{Jet}_{(\mu)}$	0.417	0.390	0.353	0.336	0.268
$R^{\mu\in Jet}_{event}$	0.019	0.019	0.019	0.017	0.014
Pt^{miss}	5.529	5.487	5.412	5.337	4.975
$Pt^{miss}_{\nu\in Jet}$	24.076	24.016	23.622	23.102	21.347
Nevent$_{(c)}$	1012	694	487	261	44
Nevent$_{(b)}$	138	90	60	27	4
$29sub/all$	0.86	0.85	0.84	0.83	0.80
R_{jet}	0.66	0.65	0.65	0.65	0.64
Entries	49253	34775	25582	14562	2786

$$300 < P_t^{\gamma} < 360\ GeV/c$$

Table 7: Selection 1. $\phi_{(\gamma,jet)} = 180^\circ \pm 15^\circ$. UA1 algorithm. $L_{int} = 3\ fb^{-1}$

Pt^{clust}_{CUT}	30	20	15	10	5
Pt^{jet}	320.158	321.502	322.289	322.869	322.911
Pt^{Jet}–Pt^{jet}	1.077	1.069	1.060	1.015	1.161
$Pt^{Jet}_{(\nu)}$	1.081	1.072	1.063	1.018	1.163
$R^{\nu\in Jet}_{event}$	0.035	0.034	0.033	0.033	0.035
$Pt^{Jet}_{(\mu)}$	0.515	0.506	0.476	0.448	0.433
$R^{\mu\in Jet}_{event}$	0.019	0.018	0.017	0.017	0.017
Pt^{miss}	5.764	5.721	5.692	5.572	5.691
$Pt^{miss}_{\nu\in Jet}$	31.983	32.597	33.078	32.371	35.201
Nevent$_{(c)}$	172	117	84	46	8
Nevent$_{(b)}$	25	15	10	6	1
$29sub/all$	0.84	0.83	0.82	0.80	0.78
R_{jet}	0.62	0.62	0.62	0.62	0.61
Entries	46297	32513	24157	14318	2642

Table 8: Selection 1. $\phi_{(\gamma,jet)} = 180^\circ \pm 15^\circ$. LUCELL algorithm. $L_{int} = 3\ fb^{-1}$

Pt^{clust}_{CUT}	30	20	15	10	5
Pt^{jet}	320.687	322.011	322.732	323.248	323.646
Pt^{Jet}–Pt^{jet}	1.072	1.061	1.055	0.983	1.052
$Pt^{Jet}_{(\nu)}$	1.076	1.064	1.057	0.985	1.053
$R^{\nu\in Jet}_{event}$	0.035	0.033	0.033	0.032	0.032
$Pt^{Jet}_{(\mu)}$	0.507	0.483	0.480	0.412	0.388
$R^{\mu\in Jet}_{event}$	0.018	0.018	0.017	0.016	0.013
Pt^{miss}	5.761	5.722	5.686	5.499	5.465
$Pt^{miss}_{\nu\in Jet}$	32.220	33.054	33.221	31.968	34.611
Nevent$_{(c)}$	161	106	74	39	7
Nevent$_{(b)}$	22	14	9	5	1
$29sub/all$	0.83	0.82	0.81	0.80	0.77
R_{jet}	0.66	0.65	0.65	0.65	0.64
Entries	43320	29783	21707	12104	2334